Dynamics of semiconductor lasers with external multicavities

Alexander Többens and Ulrich Parlitz
Drittes Physikalisches Institut, Universität Göttingen, Friedrich-Hund-Platz 1, 37077 Göttingen, Germany
(Received 24 May 2007; revised manuscript received 15 April 2008; published 21 July 2008)

Extending a semiconductor laser by means of an external resonator providing a weak optical feedback causes high-dimensional chaotic fluctuations of the light intensity. Adding a second resonator with different round-trip time may turn these fluctuations into more ordered oscillations or even lead back to a stable steady-state operation. The stability range of periodic or continuous wave solutions can be increased by adding a third resonator to the system. This stabilizing effect of multicavities is shown experimentally and theoretically using numerical simulations based on an extended Lang-Kobayashi model and corresponding linear stability analysis of continuous wave solutions.

DOI: 10.1103/PhysRevE.78.016210 PACS number(s): 05.45.Gg

I. INTRODUCTION

A semiconductor laser is commonly known as a system with extremely well-ordered dynamics. This order, however, can be destroyed by simply pointing the laser at a mirror, such that a fraction of its own light output is led back into its internal resonator [1]. The laser will start to fluctuate, and depending on a number of parameters, several interesting dynamics can occur, including high-dimensional chaos.

These phenomena, however interesting, have been known for a long time and are well studied. In 1977, Risch and Voumand were the first to describe the so-called *low-frequency fluctuations* (LFFs) of a semiconductor laser [2]. They occur for very small reflectivities and pump currents only slightly above the threshold current. The light output is then characterized by frequent and very sudden *power dropouts*, each followed by a relatively slow recreation of the light intensity. Modulated onto them is a fast oscillation that can usually only be seen low pass filtered due to the finite response time of the photodiode used to capture the intensity and limited transfer functions of subsequent amplifiers and oscilloscopes. The frequency of the power dropouts is only 3–30 MHz, which is amazingly slow compared to the fast oscillations that are in the range of several GHz.

The first model to generally describe the dynamics of semiconductor lasers with optical feedback was proposed by Lang and Kobayashi in 1980 [3]. They extended the well-known semiconductor rate equations by a feedback term, which leads to a system of equations known as the *Lang-Kobayashi equations* (LKEs) [4]:

$$\dot{E}_0(t) = \frac{1}{2} G_N n(t) E_0(t) + \kappa E_0(t-\tau) \times \cos[\omega_0 \tau + \phi(t) - \phi(t-\tau)], \tag{1a}$$

$$\dot{\phi}(t) = \frac{1}{2} \alpha G_N n(t) - \kappa \frac{E_0(t-\tau)}{E_0(t)} \times \sin[\omega_0 \tau + \phi(t) - \phi(t-\tau)], \tag{1b}$$

$$\dot{n}(t) = (p-1) J_{th} - \gamma n(t) - [\Gamma + G_N n(t)] E_0^2(t), \tag{1c}$$

where κ is the differential feedback rate. The equation for the complex electric field $E(t) = E_0(t) \exp\{i[\omega_0 t + \phi(t)]\}$ has been split into two one-dimensional real equations, and $n(t) = N(t) - N_{sol}$ is the carrier number above the value N_{sol} of the unperturbed, "solitary" semiconductor laser with no optical feedback. τ is the light round-trip time in the external resonator. All other parameters are explained in Table I. Using these equations, Lang and Kobayashi were able to simulate the phenomena they discovered for small reflectivities and laser-mirror distances of 1–2 cm, such as multistability or hysteresis, similar to a nonlinear Fabry-Perot resonator.

The origin of the LFF dynamics remained unclear for many years. Fujiwara *et al.* [6] suggested the LFFs to result from a decreased relaxation oscillation frequency. Henry and Kazarinov [7] assumed a stable resonator mode out of which the laser is randomly kicked by spontanous emission noise, causing power dropouts, and Hohl *et al.* [8] showed that the nature and statistics of the LFFs are indeed influenced by this noise. Mørk *et al.* [9] assumed the laser to become bistable due to the feedback, such that the spontanous emission noise would cause a mode hopping between these two states. In 1994, Sano [10] showed that the LFF dynamics could be simulated by the deterministic LKEs. Those simulations also revealed the frequency of the fast oscillations mentioned above. They were eventually visualized experimentally by Fischer *et al.* [11] in 1996. In 1998 Ahlers *et al.* [12] showed that chaotic LFF dynamics generated by the LKEs may possess many positive Lyapunov exponents and that this hyperchaotic dynamics can be synchronized by unidirectional optical coupling.

LFFs were generally assumed to be a phenomenon of only low pump currents, until in 1997 when Pan *et al.* [13] were the first to show both experimentally and numerically

TABLE I. Parameters used in the simulations and calculations. All values except ω_0 taken from [5].

G_N	2.142×10^{-5} ns^{-1}	Differential optical gain
α	5.0	Linewidth enhancement factor
γ	0.909 ns^{-1}	Carrier loss rate
Γ	0.357 ps^{-1}	Photon loss rate
J_{th}	1.552×10^{8} ns^{-1}	Threshold current density
p	1.02	Pump current density over J_{th}
$2\pi c/\omega_0$	682.7 nm	Solitary laser wavelength

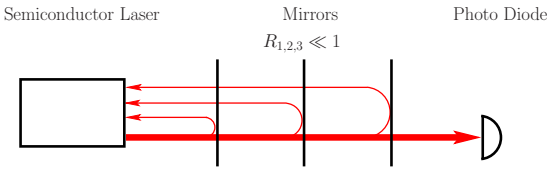

FIG. 1. (Color online) Experimental setup.

that in the case of larger feedback rates they occur for currents well above the laser threshold as well. In this regime, power dropouts turn into *power jump-ups*. They appear like inverted power dropouts, but their modeling is more complicated [14,15].

In 1994 Fischer *et al.* [16] extended a laser diode by a T-shaped external cavity with two mirrors and a beam splitter. Focusing on the special case of equal feedback rates for both mirrors and one cavity being twice as long as the other, they found periodic and chaotic solutions and studied the system's routes to chaos. Furthermore, they were able to reproduce the experimental behavior via numerical simulations. Three years later, Liu and Ohtsubo [17] investigated the same system with arbitrary cavity lengths and feedback rates. They found that there exist wide parameter ranges with stable light outputs (i.e., steady states or limit cycles) and proposed this as a method to suppress feedback-induced intensity noise. A deeper theoretical investigation was performed by Rogister *et al.* and Erneux *et al.* in 1999 [18]. They found that for a sufficient feedback rate LFF suppression takes place, however the second cavity length is chosen. In 2000, Rogister *et al.* presented an experimental confirmation of these results [19]. Detailed theoretical investigations of the possible dynamics of a system with two distant reflectors were given in 2000 by Erneux *et al.* [20], in 2002 by Sukow *et al.* [21], and in 2006 by Ruiz-Oliveras and Pisarchik [22].

II. EXTERNAL MULTICAVITIES

In the following we present the results of our observations on a laser diode with two or three distant reflectors at small pump currents. The experimental setup is shown in Fig. 1. We assume the reflectivity of each mirror to be small enough to neglect multiple reflections within or between the external cavities. In this case, the extension of the LKE for a set of M mirrors is given by

$$\dot{E}_0(t) = \frac{1}{2} G_N n(t) E_0(t) + \sum_{m=1}^{M} \kappa_m E_0(t-\tau_m) \times \cos[\omega_0 \tau_m + \phi(t) - \phi(t-\tau_m)], \tag{2a}$$

$$\dot{\phi}(t) = \frac{1}{2} \alpha G_N n(t) - \sum_{m=1}^{M} \kappa_m \frac{E_0(t-\tau_m)}{E_0(t)} \times \sin[\omega_0 \tau_m + \phi(t) - \phi(t-\tau_m)], \tag{2b}$$

$$\dot{n}(t) = (p-1) J_{th} - \gamma n(t) - [\Gamma + G_N n(t)] E_0^2(t), \tag{2c}$$

where the rates κ_m of each feedback term take into account all losses due to transmissions and reflections. Both for the two- and three-mirror systems we found a number of different dynamical regimes depending on parameter choice. Those include chaotic LFF dynamics, quasiperiodic solutions, limit cycles, and continuous wave (cw) solutions (Fig. 2), the latter being of special interest with regard to the use of external resonators to suppress feedback-induced instabilities. To find out about the effect of additional resonators on their stability, we have performed a linear stability analysis on the extended LKE.

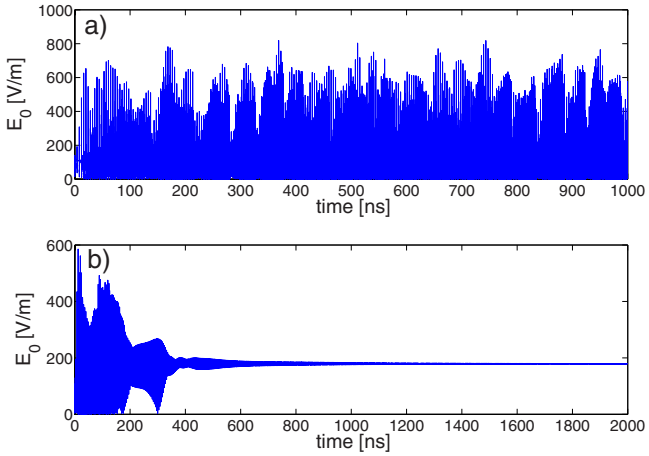

FIG. 2. (Color online) (a) LFFs in a simulation of the classical single feedback LKE with τ=4 ns and κ=50 ns^{-1}. (b) Stable cw solutions appear after a second feedback term has been added. τ_1 and κ_1 remain unchanged, τ_2=3.96 ns and κ_2=30 ns^{-1}.

On a cw solution, the field amplitude and carrier number will turn into constants and lose their time-delayed character:

$$E_0(t) = E_0(t-\tau_m) = \text{const} =: \tilde{E}_0, \tag{3a}$$

$$n(t) = n(t-\tau_m) = \text{const} =: \tilde{n}. \tag{3b}$$

The phase shift $\phi(t)$ does not become constant, but linear in time:

$$\phi(t) = \tilde{\omega} t + \phi_0, \tag{4}$$

which corresponds to a constant light frequency $\omega_0 + \tilde{\omega}$. Substituting these conditions into the extended LKE (2a)–(2c), we obtain a system of equations for the cw solutions:

$$\tilde{n} = -\frac{2}{G_N} \sum_{i=1}^{m} \kappa_m \cos(\omega_0 \tau_m + \tilde{\omega} \tau_m), \tag{5a}$$

$$\tilde{E}_0 = \sqrt{\frac{(p-1) J_{th} - \gamma \tilde{n}}{\Gamma + G_N \tilde{n}}}, \tag{5b}$$

$$\tilde{\omega} = \frac{1}{2} \alpha G_N \tilde{n} - \sum_{i=1}^{m} \kappa_m \sin(\omega_0 \tau_m + \tilde{\omega} \tau_m). \tag{5c}$$

Now that observables on a cw solution are known to us, we shall find out about their stability. Let $\mathbf{d}(t) = (\delta E_0, \delta\phi, \delta n)$ be the phase-space deviation from a cw solution. Linearizing the extended LKE (2) at the cw solution (5) and using the ansatz $\mathbf{d}(t) = e^{\lambda t} \mathbf{d}_0$, where λ is complex, leads to a system of

equations for $\mathbf{d}(t)$ (for details see the Appendix):

$$\lambda \delta E_0(t) = \frac{1}{2} G_N \tilde{E}_0 \delta n(t) - \sum_{m=1}^{M} \kappa_m [\tilde{E}_0 \sin(\omega\tau_m)(1 - e^{-\lambda\tau_m})\delta\phi(t) + \cos(\omega\tau_m)(1 - e^{-\lambda\tau_m})\delta E_0(t)], \quad (6a)$$

$$\lambda \delta\phi(t) = \frac{1}{2}\alpha G_N \delta n(t) + \sum_{m=1}^{M} \kappa_m [\tilde{E}_0^{-1} \sin(\omega\tau_m)(1 - e^{-\lambda\tau_m})\delta E_0(t) - \cos(\omega\tau_m)(1 - e^{-\lambda\tau_m})\delta\phi(t)], \quad (6b)$$

$$\lambda \delta n(t) = -2(\Gamma + G_N \bar{n})\tilde{E}_0 \delta E_0(t) - (G_N \tilde{E}_0^2 + \gamma)\delta n(t), \quad (6c)$$

where $\omega = \omega_0 + \tilde{\omega}$. The stability of a given cw solution is now defined by λ. If the real part of λ is negative, $\mathbf{d}(t)$ will converge to zero, which means stability. With $\mathbf{A}(\lambda)$ being the matrix describing the above system of equations (6a)–(6c), it is $\lambda\mathbf{d}(t) = \mathbf{A}(\lambda)\mathbf{d}(t)$. Thus λ is given by the eigenvalues of $\mathbf{A}(\lambda)$ or, equivalently, by the roots of the characteristic equation

$$\begin{aligned} 0 &= \det[\lambda\mathbf{I} - \mathbf{A}(\lambda)] \\ &= \lambda^3 + \lambda^2[2c + G_N\tilde{E}_0^2 + \gamma] \\ &\quad + \lambda[c^2 + s^2 + 2c(G_N\tilde{E}_0^2 + \gamma) + G_N\tilde{E}_0^2(\Gamma + G_N\bar{n})] \\ &\quad + (\Gamma + G_N\bar{n})\tilde{E}_0^2 G_N(c - s\alpha) + (s^2 + c^2)(G_N\tilde{E}_0^2 + \gamma), \end{aligned} \quad (7)$$

where $\mathbf{I}$ is the unit matrix and

$$c(\lambda) = \sum_{m=1}^{M} \kappa_m \cos(\omega\tau_m)(1 - e^{-\lambda\tau_m}),$$

$$s(\lambda) = \sum_{m=1}^{M} \kappa_m \sin(\omega\tau_m)(1 - e^{-\lambda\tau_m}).$$

The cw solution's stability depends on the root of Eq. (7) with the largest real value, which from now on will be called the *dominant root*, or λ_{dom}, shortly. The real part of λ_{dom} can be seen as a quantitative measure of the system's stability. The detection of λ_{dom} is not easy because Eq. (7) has an infinite number of roots. Our method was to put a sufficiently large and fine grid onto the complex plane, calculate Eq. (7) for each grid point, and start a numerical root finder at the minima.

The characteristic equation (7) has a parameter-independent root at $\lambda = 0$, because $c(0) = s(0) = 0$. This neutral eigenvalue originates from the linear phase dynamics in Eq. (4) and results in a time-independent phase shift. Since the light intensity is not affected by this phase dynamics, this vanishing eigenvalue will be ignored in the following stability analysis.

Figure 3(a) shows a stability analysis of a single feedback laser ($M=1$) for a number of feedback rates. As expected, the stable, solitary laser ($\kappa_1 = 0$) is more and more destabilized the stronger the optical feedback becomes. According to our numerical simulations the cw operation stops at $\kappa_1 = 0.18\ \mathrm{ns}^{-1}$, and after a series of Hopf bifurcations chaos sets in at $\kappa_1 = 0.55\ \mathrm{ns}^{-1}$. Even though cw solutions exist even well above that value, they are only weakly stable and their basins are too small to actually capture the phase-space trajectory. In Fig. 3(b), κ_1 is fixed to $30\ \mathrm{ns}^{-1}$ and a second feedback is added, which for certain values of the feedback rate κ_2 has a stabilizing effect.

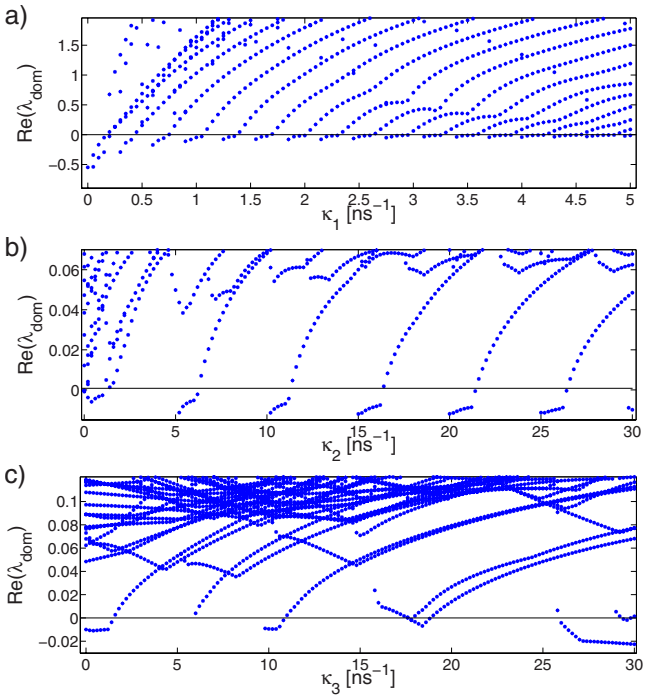

FIG. 3. (Color online) In these diagrams, each dot represents a cw solution as determined by Eqs. (5), and its vertical position gives the real part of λ_{dom}. Dots below the zero line represent stable stationary solutions. (a) Destabilization of the laser by means of a single optical feedback with $\tau_1 = 4$ ns and (b) $\kappa_1 = 30\ \mathrm{ns}^{-1}$. Adding a second feedback with $\tau_2 = 2.75$ ns with a properly chosen feedback rate κ_2 leads to a restabilization of the single feedback case ($\kappa_2 = 0$). (c) $\kappa_2 = 30\ \mathrm{ns}^{-1}$, a third feedback term with $\tau_3 = 1.27$ ns has been added. In a small regime around $\kappa_3 = 30\ \mathrm{ns}^{-1}$ the steady-state stability increases compared to the double-feedback case.

We also investigated whether it is possible to improve stability by adding a third resonator. A systematic series of stability analyses for several combinations of round-trip times and feedback rates indicated that this is indeed the case. Like the second resonator added to the single-feedback system, a third resontator may have a stabilizing or a destabilizing effect on the double-feedback system, depending on parameter choice [Fig. 3(c)]. For properly chosen values of τ_3 and κ_3 a significant increase in stability can be achieved, even though the stability remains weak compared to the unperturbed laser. The most stable stationary solution we found for a triple-feedback system had a stability of $\mathrm{Re}(\lambda_{\mathrm{dom}}) = -0.06$, where for the unperturbed laser we found $\mathrm{Re}(\lambda_{\mathrm{dom}}) = -0.55$.

III. EXPERIMENTAL RESULTS

In our experiment, installation of one or more additional resonators led to stabilization, too, as can be seen in Fig. 4.

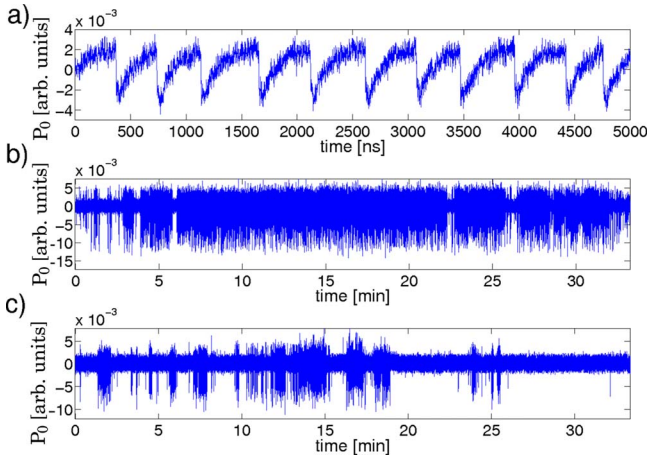

FIG. 4. (Color online) Experimental time series of the ac-coupled intensity $P_0=E_0^2-\langle E_0^2\rangle$ where $\langle E_0^2\rangle$ denotes the mean value. (a) LFF dynamics of a semiconductor laser with one external resonator with round-trip time $\tau_1=10.6$ ns. (b) Adding a second resonator with $\tau_2=9.8$ ns leads to short periods of (noisy) steady-state operation or low-amplitude oscillation. Note the different time scales. (c) Stability of the double-feedback system increases significantly after the installation of a third resonator with $\tau_3=1.47$ ns. The laser now remains stable for up to several minutes.

In contrast to the numerical solutions, however, the signal corresponding to the stabilized state still possesses a finite amplitude due to measurement and/or dynamical noise (the same noise amplitude was experimentally observed for a cw semiconductor laser without any external resonators). Furthermore, in the experiment we observed frequent breakouts (see Fig. 4 [23]), which cannot be simulated by means of the extended deterministic LKE (2). The period of time between two breakouts can add up to several minutes, so they are probably not of deterministic origin. We found two different ways to reproduce them in simulations. The first one is based on the assumption that the system is in fact stable, but not stable enough to durably withstand internal and external perturbations (like spontaneous emissions and mechanical vibrations). Figure 5 shows the same simulation as seen in Fig. 2(b), but now with dynamical noise generated by Gaussian random numbers superimposed on each system variable during integration. The result is a time series very similar to what we see in Figs. 4(b) and 4(c). In view of the results of the stability analysis this is not very surprising, because the cw solution's stability always remained very fragile compared to the solitary laser, no matter how the parameters

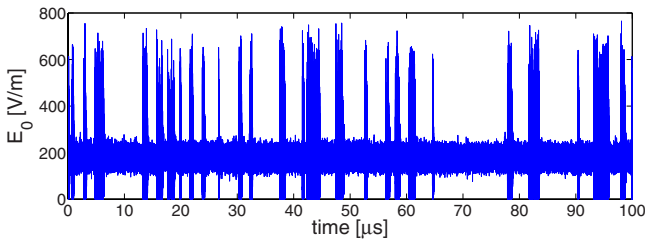

FIG. 5. (Color online) Simulation from Fig. 2(b) corrupted by dynamical noise.

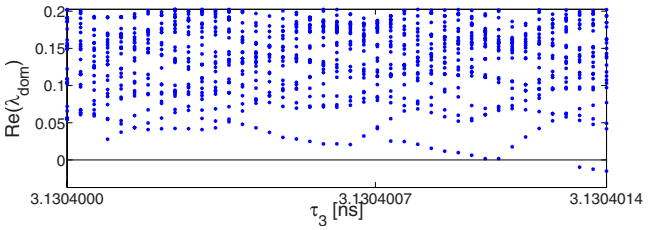

FIG. 6. (Color online) Change of stationary solutions stability with external round trip time where $\tau_1=4$ ns, $\tau_2=2.150045$ ns, and $\kappa_{1,2,3}=30$ ns^{-1}. The interval over which τ_3 is varied corresponds to a shift in the external optical path length of little more than half a wavelength.

were chosen. In the simulation the time intervals between two outbreaks are smaller that than those in the experimental time series by many orders of magnitude, because a rather strong noise signal has been used to speed up calculations (it would be too time consuming to simulate several seconds of laser dynamics). The cw operation intervals in the simulation, however, can be stretched arbitrarily by decreasing the noise amplitude.

When observing the experimental system for a long time one can observe changes in the mean frequency of breakouts and stable operation [see, for example, Fig. 4(b), where during the first 5 min more stable time intervals occur than in the following 20 min]. The system seems to be nonstationary on a slow time scale (minutes). There is strong evidence that this nonstationarity is caused by small fluctuations of the external resonator lengths due to thermal effects or mechanical perturbations. In certain regions of parameter space there is a very sensitive dependence of dynamics and stability with respect to the delay times τ_m as can be seen in Fig. 6. Cavity length shifts of less than a wavelength may push the system from a stable into an unstable regime or vice versa. According to our analytical investigations by means of steady-state analysis, we found that the density of stable steady-state solutions increases for small values of τ_2 and τ_3. Accordingly, best stabilizing effects in the experiment were achieved for small lengths of the additional cavities.

We have run a simulation with two feedback terms and a sinosoidal fluctuation of τ_2 (Fig. 7). Again, the result is very similar to what we see in our experimental time series. Depending on the current value of the second round-trip time, the system changes between two different attractors. The oscillation amplitude of τ_2 is 3×10^{-4} ns, which corresponds to an optical path length shift of 0.09 mm. Note that no noise has been added to this time series. The dynamics between the outbreaks does not represent a noise-corrupted steady-state solution, as is the case in Fig. 5, but a real low-amplitude solution of the extended LKE. Experimentally these two cases are difficult to distinguish. However, in the case of steady-state operation the amplitude between the outbreaks should be equal to the (noisy) amplitude measured for the solitary laser without external feedback. This has been the case for some of our measured time series, which indicates that actually steady-state operation has been realized in our experiments.

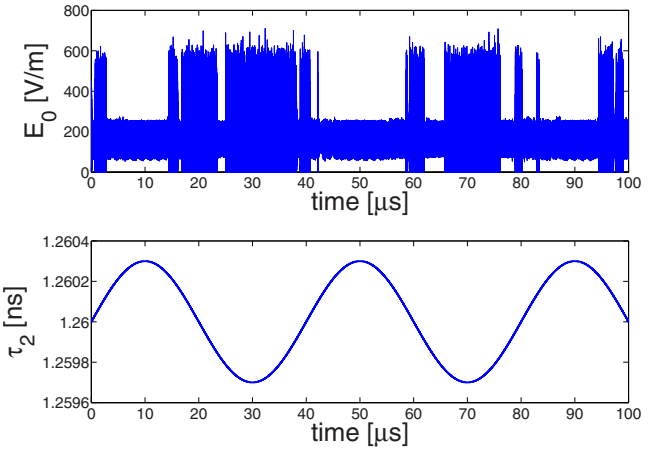

FIG. 7. (Color online) (a) Simulation of the extended LKE with double feedback where τ_2 is time dependent, $\tau_1=4$ ns, $\kappa_1=30$ ns^{-1}, and $\kappa_2=36.5$ ns^{-1}. (b) Current value of τ_2.

IV. CONCLUSIONS

We have shown that stabilization of chaotic semiconductor laser with an external resonator by means of a second external resonator can be enhanced by adding a third resonator to the system. However, the resulting cw solutions are only weakly stable, and in addition an extremely sensitive dependence of system dynamics from the external optical path length exists in certain regions of parameter space. Therefore it is difficult to achieve durable stationary laser operation experimentally. A linear stability analysis of cw solutions of an extended Lang-Kobayashi equation confirms this phenomenon, including the amount of (weak) stability achieved, its sensitive dependence on the lengths of the resonator(s) and the accumulation of stable steady state solutions in the regime of small round trip times. Experiment and simulation are in good accordance when dynamical noise and/or time-dependent cavity lenghts are included. We conjecture that the observed stabilizing effect of multiple delayed feedback is a general feature of dynamical systems or networks [24–26].

APPENDIX: STABILITY OF STEADY-STATE SOLUTIONS

The extended Lang-Kobayashi equations (2) can be written as follows:

$$\dot{x}(t) = g[x(t)] + \sum_{m=1}^{M} \kappa_m h[x(t), x(t-\tau_m)], \tag{A1}$$

where

$$g[x(t)] = \begin{pmatrix} \frac{1}{2} G_N n(t) E_0(t) \\ \frac{1}{2} \alpha G_N n(t) \\ (p-1) J_{th} - \gamma n(t) - [\Gamma + G_N n(t)] E_0^2(t) \end{pmatrix} \tag{A2}$$

and

$$h[x(t), x(t-\tau_m)] = \begin{pmatrix} E_0(t-\tau_m)\cos[\omega_0 \tau_m + \phi(t) - \phi(t-\tau_m)] \\ -\frac{E_0(t-\tau_m)}{E_0(t)} \sin[\omega_0 \tau_m + \phi(t) - \phi(t-\tau_m)] \\ 0 \end{pmatrix}. \tag{A3}$$

The phase-space deviation from a given trajectory $y(t)$ is $d(t)=x(t)-y(t)$ and is described by the following differential equations:

$$\dot{d}(t) = \dot{x}(t) - \dot{y}(t) = g[x(t)] - g[y(t)] + \sum_{m=1}^{M} \kappa_m \{h[x(t), x(t-\tau_m)] - h[y(t), y(t-\tau_m)]\}. \tag{A4}$$

After linearization we obtain

$$\dot{d}(t) = Dg[x(t)] d(t) + \sum_{m=1}^{M} \kappa_m Dh[x(t), x(t-\tau_m)](d(t), d(t-\tau_m)). \tag{A5}$$

where Dg and Dh are Jacobians and the vectors $d(t)$ and $(d(t), d(t-\tau_m))$ are defined by

$$d(t) = \begin{pmatrix} \delta E_0(t) \\ \delta \phi(t) \\ \delta n(t) \end{pmatrix} \tag{A6}$$

and

$$(d(t), d(t-\tau_m)) = \begin{pmatrix} \delta E_0(t) \\ \delta \phi(t) \\ \delta n(t) \\ \delta E_0(t-\tau_m) \\ \delta \phi(t-\tau_m). \end{pmatrix}. \tag{A7}$$

Using the abbreviation $\Phi(t)=\omega_0 \tau_m + \phi(t) - \phi(t-\tau_m)$, Jacobians are as follows:

$$Dg[x(t)] = \begin{pmatrix} \frac{1}{2} G_N n(t) & 0 & \frac{1}{2} G_N E_0(t) \\ 0 & 0 & \frac{1}{2} \alpha G_N \\ -2[\Gamma + G_N n(t)] E_0(t) & 0 & -G_N E_0(t)^2 - \gamma \end{pmatrix}, \tag{A8}$$

$$Dh[x(t),x(t-\tau_m)] = \begin{pmatrix} 0 & -E_0(t-\tau_m)\sin[\Phi(t)] & 0 & \cos[\Phi(t)] & E_0(t-\tau_m)\sin[\Phi(t)] \\ \frac{E_0(t-\tau_m)}{E_0(t)^2}\sin[\Phi(t)] & -\frac{E_0(t-\tau_m)}{E_0(t)}\cos[\Phi(t)] & 0 & -\frac{1}{E_0(t)}\sin[\Phi(t)] & \frac{E_0(t-\tau_m)}{E_0(t)}\cos[\Phi(t)] \\ 0 & 0 & 0 & 0 & 0 \end{pmatrix}. \tag{A9}$$

Using Eqs. (3) and (4) leads to a system of equations

$$\delta\dot{E}_0(t) = \frac{1}{2}G_N\tilde{n}\,\delta E_0(t) + \frac{1}{2}G_N\tilde{E}_0\delta n(t) - \sum_{m=1}^{M}\{\kappa_m\tilde{E}_0\sin(\omega\tau_m)[\delta\phi(t)-\delta\phi(t-\tau_m)] - \kappa_m\cos(\omega\tau_m)\delta E_0(t-\tau_m)\}, \tag{A10a}$$

$$\delta\dot{\phi}(t) = \frac{1}{2}\alpha G_N\delta n(t) + \sum_{m=1}^{M}\left(\frac{\kappa_m}{\tilde{E}_0}\sin(\omega\tau_m)[\delta E_0(t)-\delta E_0(t-\tau_m)] - \kappa_m\cos(\omega\tau_m)[\delta\phi(t)-\delta\phi(t-\tau_m)]\right), \tag{A10b}$$

$$\delta\dot{n}(t) = -2(\Gamma + G_N\tilde{n})\tilde{E}_0\delta E_0(t) - (G_N\tilde{E}_0^2 + \gamma)\delta n(t), \tag{A10c}$$

where $\omega=\omega_0+\tilde{\omega}$. Substituting the relation (5a) into (A10a) turns it to

$$\delta\dot{E}_0(t) = \frac{1}{2}G_N\tilde{E}_0\delta n(t) - \sum_{m=1}^{M}\{\kappa_m\tilde{E}_0\sin(\omega\tau_m)[\delta\phi(t)-\delta\phi(t-\tau_m)] + \kappa_m\cos(\omega\tau_m)[\delta E_0(t)-\delta E_0(t-\tau_m)]\}. \tag{A11}$$

Using the ansatz

$$d(t) = e^{\lambda t}d_0, \quad \lambda\in\mathbb{C}, \tag{A12}$$

the system takes the following form:

$$\lambda\,\delta E_0(t) = \frac{1}{2}G_N\tilde{E}_0\delta n(t) - \sum_{m=1}^{M}\{\kappa_m\tilde{E}_0\sin(\omega\tau_m)(1-e^{-\lambda\tau_m})\delta\phi(t) + \kappa_m\cos(\omega\tau_m)(1-e^{-\lambda\tau_m})\delta E_0(t)\}, \tag{A13a}$$

$$\lambda\,\delta\phi(t) = \frac{1}{2}\alpha G_N\delta n(t) + \sum_{m=1}^{M}\left(\frac{\kappa_m}{\tilde{E}_0}\sin(\omega\tau_m)(1-e^{-\lambda\tau_m})\delta E_0(t) - \kappa_m\cos(\omega\tau_m)(1-e^{-\lambda\tau_m})\delta\phi(t)\right), \tag{A13b}$$

$$\lambda\,\delta n(t) = -2(\Gamma + G_N\tilde{n})\tilde{E}_0\delta E_0(t) - (G_N\tilde{E}_0^2 + \gamma)\delta n(t). \tag{A13c}$$

[1] J. Ohtsubo, *Semiconductor Lasers—Stability, Instability and Chaos, Springer Series in Optical Sciences* (Springer-Verlag, Berlin, 2006).
[2] C. Risch and C. Voumand, J. Appl. Phys. **48**, 2083 (1977).
[3] R. Lang and K. Kobayashi, IEEE J. Quantum Electron. **16**, 347 (1980).
[4] We neglect here stochastic terms due to spontaneous emission and consider a purely deterministic Lang-Kobayashi model.
[5] G. H. M. van Tartwijk, A. M. Levine, and D. Lenstra, IEEE J. Sel. Top. Quantum Electron. **1**, 466 (1995).
[6] M. Fujiwara, K. Kubota, and R. Lang, Appl. Phys. Lett. **38**, 217 (1981).
[7] C. H. Henry and R. F. Kazarinov, IEEE J. Quantum Electron. **22**, 294 (1986).
[8] A. Hohl, H. J. C. van der Linden, and R. Roy, Opt. Lett. **20**, 2396 (1995).
[9] J. Mørk, B. Tromborg, and P. L. Christiansen, IEEE J. Quantum Electron. **24**, 123 (1988).
[10] T. Sano, Phys. Rev. A **50**, 2719 (1994).
[11] I. Fischer, G. H. M. van Tartwijk, A. M. Levine, W. Elsässer, E. Göbel, and D. Lenstra, Phys. Rev. Lett. **76**, 220 (1996).
[12] V. Ahlers, U. Parlitz, and W. Lauterborn, Phys. Rev. E **58**, 7208 (1998).
[13] M.-W. Pan, B.-P. Shi, and G. Gray, Opt. Lett. **22**, 166 (1997).
[14] P. S. Spencer and K. A. Shore, Quantum Semiclassic. Opt. **9**, 819 (1997).
[15] I. Wedekind and U. Parlitz, Int. J. Bifurcation Chaos Appl. Sci. Eng. **18**, 1199 (2008).
[16] I. Fischer, O. Hess, W. Elsässer, and E. Göbel, Phys. Rev. Lett. **73**, 2188 (1994).
[17] Y. Liu and J. Ohtsubo, IEEE J. Quantum Electron. **33**, 1163 (1997).
[18] T. Erneux, F. Rogister, P. Mégret, O. Deparis, and M. Blondel, Opt. Lett. **24**, 1218 (1999).

[19] F. Rogister, D. W. Sukow, A. Gavrielides, P. Mégret, O. Deparis, and M. Blondel, Opt. Lett. **25**, 808 (2000).
[20] T. Erneux, F. Rogister, A. Gavrielides, and V. Kovanis, Opt. Commun. **183**, 467 (2000).
[21] D. W. Sukow, M. C. Hegg, and J. L. Wright, Opt. Lett. **27**, 827 (2002).
[22] F. R. Ruiz-Oliveras and A. N. Pisarchik, Opt. Express **14**, 12859 (2006).
[23] Note that the period of time shown in Fig. 4(a) in [19] is rather short compared to the typical time span between breakouts observed in our experiment.
[24] A. Ahlborn and U. Parlitz, Phys. Rev. Lett. **93**, 264101 (2004).
[25] A. Ahlborn and U. Parlitz, Phys. Rev. E **72**, 016206 (2005).
[26] C. Masoller and A. C. Martí, Phys. Rev. Lett. **94**, 134102 (2005).